Radiation Measurements 45 (2010) 497–499

Contents lists available at ScienceDirect

Radiation Measurements

journal homepage: www.elsevier.com/locate/radmeas

Red persistent luminescent silicate nanoparticles

A. Lecointre [a,*], A. Bessière [a,b], B. Viana [a], D. Gourier [a]

[a] Ecole Nationale Supérieure de Chimie de paris (Chimie ParisTech), Laboratoire de Chimie de la Matière Condensée de Paris (UMR 7574 CNRS), 11 Rue P&M Curie, 75231 Paris Cedex 05, France
[b] Goa University, Physics Group, Taleigao Plateau, Goa, India, 403206

ARTICLE INFO

Article history:
Received 15 August 2009
Received in revised form
7 January 2010
Accepted 31 January 2010

Keywords:
Diopside nanoparticles
Persistent luminescence
Thermally stimulated luminescence

ABSTRACT

Red persistent luminescent diopside nanoparticles doped with Mn^{2+} and codoped with RE^{3+} (Eu^{2+}, Dy^{3+}) have been obtained by sol-gel method. The influence of codoping rare earth ions on the persistent luminescence was studied by wavelength-resolved thermally stimulated luminescence (TSL) measurements from 30 to 650 K after X-ray irradiation. From these first results, a mechanism of persistent luminescence is proposed. In this mechanism Mn^{2+} and Eu^{2+} act as TSL recombination centers, Mn^{3+} and Eu^{3+} being stable hole centers, whereas Dy^{3+} acts as a good electron trap giving rise to a TSL peak at high temperature. Finally, persistent luminescence was measured. Intensity and persistence of the red luminescence of $CaMgSi_2O_6$: Mn^{2+}–Dy^{3+} are better than those of $CaMgSi_2O_6$: Mn^{2+} and $CaMgSi_2O_6$: Mn^{2+}–Eu^{2+}, which are in agreement with the results of TSL.

1. Introduction

We have recently developed inorganic luminescent nanoparticles ($Ca_{0.2}Zn_{0.9}Mg_{0.9}Si_2O_6$: Eu^{2+}, Mn^{2+}, Dy^{3+}), which are suitable for *in vivo* imaging and can avoid most of inherent problems encountered in classical optical systems (Le Masne de Chermont et al., 2007). The key element of this technology is based on persistent luminescence nanoparticles emitting in the red to near-infrared, which can be optically excited before injection. The persistent luminescence lasts for several hours and permits the removal of the background noise originating from *in situ* excitation ("autofluorescence" of tissues (Frangioni, 2003)). Thus, the significant signal-to-noise ratio improvement allows detection in deep organs of small animals and real-time biodistribution monitoring of active elements hours after injection.

In the aim of understanding the persistent luminescence mechanism involved in these nanoparticles and improving their properties, the binary compound $CaMgSi_2O_6$ with the same structure (diopside) as $Ca_{0.2}Zn_{0.9}Mg_{0.9}Si_2O_6$ was studied with different dopants. Wavelength-resolved thermally stimulated luminescence (TSL) measurements from 30 to 650 K after X-ray irradiation were performed on $CaMgSi_2O_6$: Mn^{2+}, $CaMgSi_2O_6$: Mn^{2+}–Eu^{2+} and $CaMgSi_2O_6$: Mn^{2+}–Dy^{3+}.

2. Experimental

Powder samples were prepared by a sol-gel process. The raw materials are $Mg(NO_3)_2.6H_2O$, $CaCl_2.2H_2O$, $ZnCl_2$, $MnCl_2$, $EuCl_3.6H_2O$, $DyNO_3.5H_2O$ and $(CH_3CH_2O)_4Si$ (TEOS). The nominal concentrations of Eu^{2+}, Dy^{3+} and Mn^{2+} were respectively 1.0%, 1.0% and 2.5% relative to the $(Ca^{2+} + Mg^{2+})$ amount. The salts were dissolved in deionized water acidified at pH 2 by addition of nitric acid. TEOS was then added rapidly, and the solution was stirred vigorously at room temperature for 3 h. The solution was heated at 70 °C for 2 h until the sol-gel transition occurred. The wet gel was then dried at 120 °C for 20 h, and sintered at 1000 °C for 8 h under reducing atmosphere.

X-rays diffraction (XRD) patterns were obtained on an X'PERT PRO X-ray diffractometer working with Cu Kα radiation. Fluorescence spectrum was measured with a varian Cary Eclipse Fluorescence Spectrophotometer. Radio-luminescence (RL) measurement was carried out under X-rays from a molybdene tube operating at 50 kV, 20 mA. TSL experiments were recorded after 10 min irradiation with X-rays, with a heating rate of 10 K/min from 30 K to 650 K. Persistent luminescence spectra were measured after 10 min irradiation with X-rays. For RL, TSL and persistent luminescence, light was collected *via* an optical fiber by a Princeton CCD camera cooled at −70 °C coupled with an Acton SpectraPro monochromator.

3. Results and discussion

The samples structure was checked by XRD (Fig. 1). Nearly all of the peaks can be attributed to diopside $CaMgSi_2O_6$ phase. Only

* Corresponding author.
E-mail address: aurelie-lecointre@enscp.fr (A. Lecointre).

1350-4487/$ – see front matter © 2010 Elsevier Ltd. All rights reserved.
doi:10.1016/j.radmeas.2010.01.043

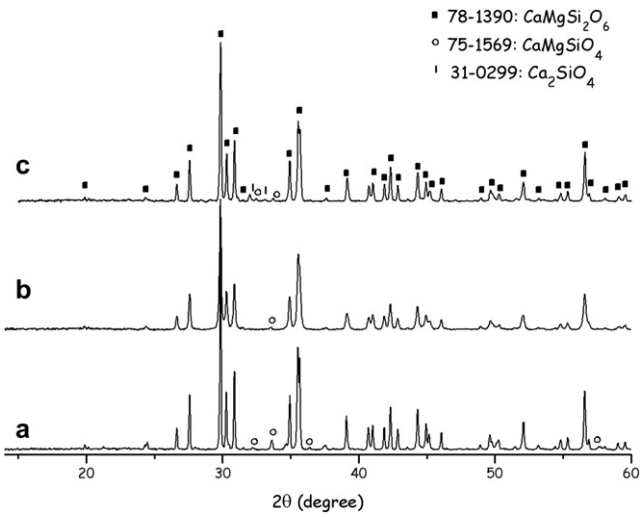

Fig. 1. XRD patterns of $CaMgSi_2O_6$: Mn^{2+} (a), $CaMgSi_2O_6$: Mn^{2+}–Eu^{2+} (b), and $CaMgSi_2O_6$: Mn^{2+}–Dy^{3+} (c).

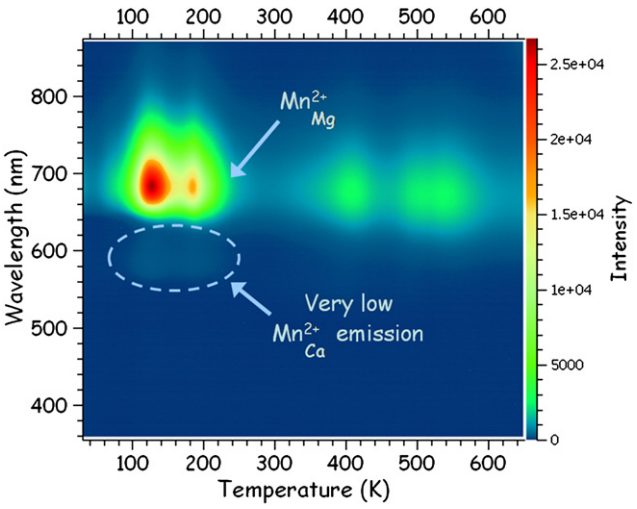

Fig. 3. Wavelength-resolved TSL spectrum of $CaMgSi_2O_6$: Mn^{2+}.

small amounts of impurity phases have been found corresponding to $CaMgSiO_4$ and Ca_2SiO_4. The particles sizes analyzed by transmission electron microscopy were found to be between 50 and 200 nm.

The two emission bands of Mn^{2+} in $CaMgSi_2O_6$:Mn^{2+} at 580 and 680 nm are shown in Fig. 2. These two broad bands are attributed to the same $^4T_1$–$^6A_1$ transition of Mn^{2+} in two different surroundings. Indeed $CaMgSi_2O_6$ possesses two different octahedral cationic sites: a small one M1 occupied by Mg^{2+} and a large one M2 occupied by Ca^{2+}. The ionic radius of Mn^{2+} (in six-fold coordination) is 0.83 Å whereas the radii of Mg^{2+} and Ca^{2+} are 0.72 Å and 1.00 Å, respectively (Shannon and Prewitt, 1969). As Mn^{2+} has an intermediate size between the two cations, it occupies both Ca and Mg sites. When Mn^{2+} susbtitutes Mg^{2+}, i.e. occupies the smallest cationic site of the structure, the crystal field around Mn^{2+} is stronger than when Mn^{2+} substitutes Ca^{2+}. From the Tanabe–Sugano diagram for a d^5 ion (Tanabe and Sugano, 1954), the emission at longer wavelength (680 nm) can be attributed to the $^4T_1$–$^6A_1$ transition of Mn^{2+} in the strongest crystal field, i.e. to Mn in substitution of Mg. In the same way, the emission at 580 nm is attributed to the $^4T_1$–$^6A_1$ transition of Mn^{2+} in Ca site (weaker crystal field).

The fluorescence spectrum at room temperature under excitation in the $^6A_1$- (^4E,$^4A_1$) absorption transitions of Mn^{2+} at 412 nm (which are independent of the crystal field strength, i.e. non selective excitation of Mn^{2+} ions) is shown in Fig. 2(a). It can be seen that Mn^{2+} emission is stronger in Ca site than in Mg site, indicating that the former site is more populated than the latter.

The persistent luminescence spectrum at room temperature recorded after switching off the X-ray excitation (Fig. 2(b)) exhibits mostly the emission of Mn^{2+} in Mg site. This shows that the emission mechanism of persistent luminescence is different from the one of fluorescence. An intermediate situation occurs under X-ray excitation (Fig. 2(c)) where the emission of Mn^{2+} in Ca site is much weaker than the one of fluorescence.

The wavelength-resolved TSL spectrum of $CaMgSi_2O_6$: Mn^{2+} is presented in Fig. 3. Two strong peaks are observed at low temperature (corresponding to shallow traps) and two weaker peaks appear at higher temperature. Emissions corresponding to all these TSL peaks are mostly located at 680 nm, which means that they originate almost exclusively from Mn^{2+} in Mg site. The similarity of the TSL emission and the persistent luminescence spectrum shows that the same mechanism should occur.

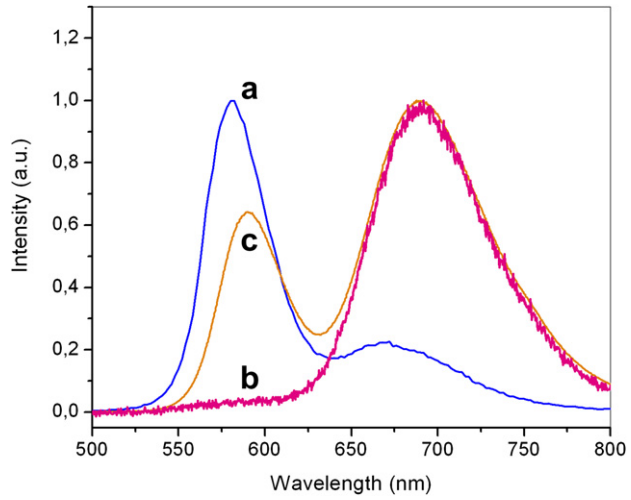

Fig. 2. $^4T_1$–$^6A_1$ optical emission of Mn^{2+} in $CaMgSi_2O_6$: Mn^{2+}. (a) fluorescence spectrum, (b) Persistent luminescence spectrum, (c) RL spectrum.

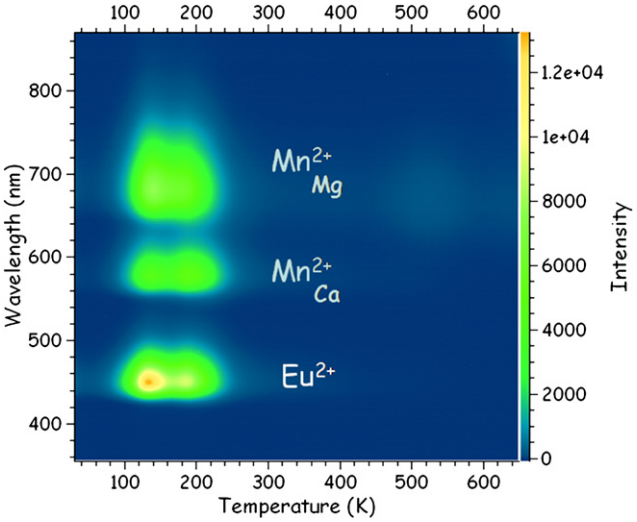

Fig. 4. Wavelength-resolved TSL spectrum of $CaMgSi_2O_6$: Mn^{2+}–Eu^{2+}.

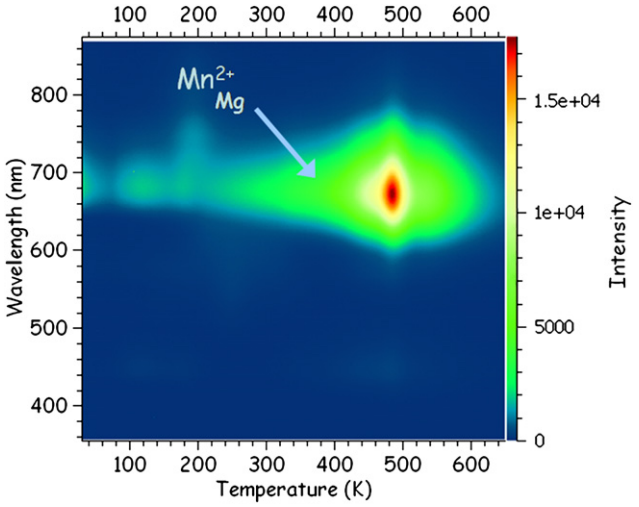

Fig. 5. Wavelength-resolved TSL spectrum of $CaMgSi_2O_6$: Mn^{2+}–Dy^{3+}.

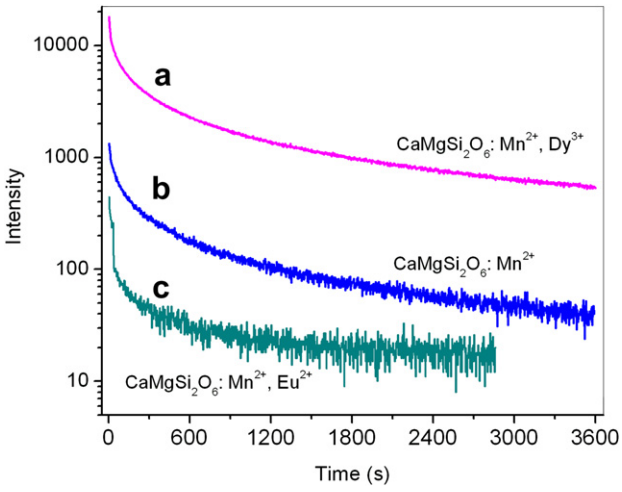

Fig. 6. Persistent luminescence spectra at 680 nm: (a) $CaMgSi_2O_6$: Mn^{2+}–Dy^{3+}, (b) $CaMgSi_2O_6$: Mn^{2+}, (c) $CaMgSi_2O_6$: Mn^{2+}–Eu^{2+}.

The luminescent center Mn^{2+} may act as a hole trap in this compound ($Mn^{2+} + h^+ \rightarrow Mn^{3+}$) and, in particular, Mn^{2+} in Mg site appears as a much better hole trap than Mn^{2+} in Ca site. In this case, the TSL peaks are related to electron traps which might be intrinsic defects in the lattice. We have tested this hypothesis by doping the material with Eu^{2+} and Dy^{3+}, which can act as hole and electron traps respectively.

The TSL spectrum of $CaMgSi_2O_6$: Mn^{2+}–Eu^{2+} is displayed in Fig. 4. At low temperature, peaks position appears at the same temperature meaning that the same electron traps are involved but the emission spectra changed. Indeed, the emission of Mn^{2+} in Mg site at 680 nm is still observed (with lower intensity) but also the emission of Mn^{2+} in Ca site at 580 nm and the emission of Eu^{2+} at 450 nm with higher intensity. In this compound, Eu^{2+} also plays the role of hole trap ($Eu^{2+} + h^+ \rightarrow Eu^{3+}$) and appears as the favored recombination center in low temperature TSL. After recombination of the electron with Eu^{3+} ($Eu^{3+} + e^- \rightarrow Eu^{2+*}$), the excited Eu^{2+} transfers its energy to the two different Mn^{2+}, which explains why both Mn^{2+} emission bands are observed in this case.

The TSL spectrum of $CaMgSi_2O_6$: Mn^{2+}–Dy^{3+} is shown in Fig. 5. Firstly, only the emission of Mn^{2+} in Mg site is observed and no luminescence of Dy^{3+} appears, meaning that Dy^{3+} does not play the role of recombination center. Moreover, unlike Mn^{2+}–Eu^{2+}-doped compound, the addition of Dy^{3+} strongly modifies the TSL peaks position. Peaks at low temperature are much weaker whereas a new broad peak with high intensity appears around 480 K. This means that Dy^{3+} plays the role of a deeper electron trap ($Dy^{3+} + e^- \rightarrow Dy^{2+}$) than intrinsic electron traps in the mechanism.

Finally persistent luminescence of Mn^{2+} in Mg site (emission at 680 nm) was measured for an hour. The Mn^{2+}–Dy^{3+}-doped compound shows a much stronger persistent luminescence than the two others (Fig. 6). $CaMgSi_2O_6$:Mn^{2+}–Dy^{3+} appears to be a good persistent luminescence phosphor for *in vivo* small animal imaging whereas $CaMgSi_2O_6$:Mn^{2+} and $CaMgSi_2O_6$:Mn^{2+}–Eu^{2+} do not. The effect of Dy^{3+} which creates new high temperature peak at 480 K explains the better persistent luminescence observed. Indeed the low temperature tail of the glow peak at 480 K is in the region of interest for persistent luminescence (between 300 and 420 K). In the Mn^{2+}–Eu^{2+}-doped compound, the quenching of the red persistent luminescence is due to the competition between Eu^{2+} and Mn^{2+} ions to trap a hole.

4. Conclusions

Diopside nanoparticles doped with Mn^{2+} and codoped with RE^{3+} (Eu^{2+}, Dy^{3+}) were prepared by sol-gel method. The Mn^{2+}-doped compound presents two broad bands at 580 and 680 nm which are attributed to emissions of Mn^{2+} in Ca site and Mn^{2+} in Mg site, respectively. TSL emission spectra of $CaMgSi_2O_6$: Mn^{2+} show almost exclusively the emission of Mn^{2+} in Mg site meaning that Mn^{2+} in Mg site acts as the favored hole trap in the mechanism. Eu^{2+} and Dy^{3+} have been shown to act as hole and electron trap, respectively. The Mn^{2+}–Dy^{3+} doped compound reveals a better red persistent luminescence resulting from the creation of a deeper electron trap related to Dy^{3+}. To go into more detail about the mechanism, the energy levels position of the two types of Mn^{2+} should be determined, other codopants will be tested and finally other TSL experiments and modeling will be carried out.

Acknowledgments

This work was supported by Medicen and the Natlurim ANR project.

References

Frangioni, J., 2003. In vivo near-infrared fluorescence imaging. Curr. Opin. Chem. Biol. 7, 626–634.
Masne, Le, et al., 2007. Nanoprobes with near-infrared persistent luminescence for in vivo imaging. Proc. Natl. Acad. Sci. 104, 9266–9271.
Shannon, R.D., Prewitt, C.T., 1969. Effective ionic radii in oxides and fluorides. Acta Crystallogr. B25, 925–946.
Tanabe, Y., Sugano, S., 1954. On the absorption spectra of complex ions I. J. Phys. Soc. Jpn. 9, 753–766.